photonics

MDPI

Communication

Response of Lead Fluoride (PbF_2) Crystal under X-ray and Gamma Ray Radiation

Vasileios Ntoupis [1], Dionysios Linardatos [1], George Saatsakis [1,2], Nektarios Kalyvas [1], Athanasios Bakas [3], George Fountos [1], Ioannis Kandarakis [1], Christos Michail [1,*] and Ioannis Valais [1]

[1] Radiation Physics, Materials Technology and Biomedical Imaging Laboratory, Department of Biomedical Engineering, University of West Attica, Ag. Spyridonos, 12210 Athens, Greece
[2] Department of Biomedical Engineering, Aretaieio University Hospital, National and Kapodistrian University of Athens, Vasilissis Sofias, 11528 Athens, Greece
[3] Department of Biomedical Sciences, University of West Attica, Ag. Spyridonos, 12210 Athens, Greece
* Correspondence: cmichail@uniwa.gr

Abstract: Background: In this research, the response of a 10 × 10 × 10 mm^3 commercially available PbF_2 crystal was experimentally assessed under X-ray and gamma ray radiation to verify the possible application of this material in X-ray medical imaging. Methods: The measurements were performed under X-ray from 50 to 130 kVp and gamma ray excitation (Tc-99m 140 keV and I-131 365 keV). The PbF_2 response was experimentally assessed by the determination of the absolute luminescence efficiency (AE), X-ray luminescence efficiency (XLE), and the stopping power of this scintillating crystal in terms of the energy absorption efficiency (EAE). The results were compared with bismuth germanate (BGO) crystal, which is commonly used in medical imaging modalities. Results: The AE of PbF_2 gradually decreased from 50 kVp up to 130 kVp. The maximum value was 0.61 efficiency units (EU) at 140 keV, and the minimum value was 0.03 EU at 71 keV (130 kVp). Similarly, low values appeared for the XLE, where the maximum value was 16.9 × 10^{-5} at 140 keV. Conclusions: These findings show that the PbF_2 scintillator has unacceptably low luminescence efficiency. Although PbF_2 can effectively absorb radiation, the scintillation light, at room temperatures, is negligible, and, thus, it could not be used in medical imaging applications in the examined energy range.

Keywords: radiation sensors; medical detectors; scintillators; crystals; lead fluoride

Citation: Ntoupis, V.; Linardatos, D.; Saatsakis, G.; Kalyvas, N.; Bakas, A.; Fountos, G.; Kandarakis, I.; Michail, C.; Valais, I. Response of Lead Fluoride (PbF_2) Crystal under X-ray and Gamma Ray Radiation. *Photonics* **2023**, *10*, 57. https://doi.org/10.3390/photonics10010057

Received: 9 December 2022
Revised: 29 December 2022
Accepted: 3 January 2023
Published: 4 January 2023

1. Introduction

Scintillators have been extensively examined in recent years with respect to a number of applications in high-energy physics, security systems, geophysical exploration, astrophysics laboratories, and, mainly, in medical diagnostics [1–4]. These radiation detection materials convert energy absorbed by X and γ radiation in sparks, i.e., photons of the optical region [5,6]. The most common inorganic scintillators are LSO, BGO, LYSO, YAP, NaI(Tl), CsI(Tl), CsI(Na), $CdWO_4$, and GAGG, and they have been well investigated. However, the list of inorganic scintillators is growing every year, and researchers all over the world are trying to develop new, heavy, non-hygroscopic scintillator materials which will have low production costs [7–11]. Inorganic scintillators are applied in various modalities of medical diagnostics: positron emission tomography (PET), single-photon emission computed tomography (SPECT), mammography, thermography, elastography, electrocardiography (ECG), etc. [12–16].

Medical imaging prioritizes limiting exposure to ionizing radiation to the lowest possible levels, as is recommended by the As Low As Reasonably Achievable (ALARA) principle [17]. However, the rapid development of medical imaging modalities sets new demands on scintillator properties. More specifically, scintillator properties such as rapid decay time are very significant for time-of-flight (TOF) applications in PET [18–20].

The accurate registration of the coincidence gamma photons is defined by the coincidence time resolution (CTR) of the detector. Nowadays, the shortest CTR reported value for a commercial device is 214 picoseconds (ps), when most of the devices on the market have CTR values from 310 ps to 400 ps [21–23]. The achievement of a 10 ps CTR limit will permit major improvement in TOF-PET performance. This will result in an increase in the accuracy and in the radiopharmaceutical factor to the millimeter and enhance the signal-to-noise ratio [24]. Therefore, during the past decades, investigation and progress of fast scintillators is on the rise [25]. Moreover, timing resolution will improve if gamma ray detection can be improved using Cherenkov light, produced by charged particles moving in a transparent material with velocities greater than 3×10^8 m/s in the medium [26–28].

Fluoride single crystals have a broad transparency spectrum starting from the vacuum ultraviolet (VUV) to the infrared (IR) area. Furthermore, these crystals have several possibilities as VUV and IR scintillators [29].

Among the fluoride single crystals, a PbF_2 single crystal was selected as a possible scintillator for medical imaging [30]. The PbF_2 crystal is visually transparent, starting from 0.25 μm up to 15 μm, and its thermal conductivity (28 W/m/K) is very high [7]. The candidate crystal (PbF_2) has a huge advantage over formal scintillator materials, i.e., the large atomic number of lead (Pb) (Z = 82) increases the probability of a photoelectric effect [28]. For that reason, the absorption of all gamma ray energy in a unique interaction within the scintillator material also shows an increased probability [29]. Additionally, it is very dense (7.77 g/cm^3) and has a very high photoelectric fraction, 46%, which, in turn, provides great stopping power for the 511 KeV photons [30]. PbF_2 is an extremely successful gamma ray absorber due to its high Z and density [31,32]. The recovery time of PbF_2 under the exposure of gamma rays (105 Gy for 14 days) has been estimated in the work of Kozma et al. from measurements of transmission spectra in the order of a few days [33].

It is a very fast material (decay time–6 and 30 ns) with a very low (0.93 cm) radiation length and a 2.2 cm Moliere radius [31]. The X-ray luminescence of orthorhombic PbF_2 has been previously reported at room temperatures, even with low energy excitation (30–50 kV) [32,33]. Furthermore, it is a low-cost material with a melting point of 822 °C [10]. These properties make PbF_2 a potential candidate for radiation detection, since a fine crystal (about 10 mm thick) will reduce the dispersion and the trajectory length of photons [34].

In this research, the luminescence efficiency (AE) of a cubic 10 mm commercially available PbF_2 single crystal was examined to investigate the efficiency of this medium in detecting ionizing radiation for X-ray and gamma ray medical radiographic applications. Excitation was experimentally measured for X-ray voltages from 50 to 130 kVp (X-ray radiography) and gamma rays (Tc-99m at 140 keV and I-131 at 365 keV). The PbF_2 response was experimentally assessed by the determination of the AE (describing the light output power per incident X-ray exposure). Additionally, X-ray luminescence efficiency (XLE) was examined, and, finally, the stopping power of this scintillating crystal was calculated via the energy absorption efficiency (EAE).

2. Materials and Methods

For the current research, a cubic PbF_2 polished crystal was purchased (Advatech, London, UK) [34]. Dimensions of the crystal were $10 \times 10 \times 10$ mm^3.

2.1. Calculations

Energy Absorption Efficiency (EAE)

Energy absorption efficiency is expressed by the percentage of incident X-ray energy absorbed in the examined crystal. In our investigation, this energy fraction was defined as a function of X-ray tube voltage (in kVp). EAE is determined by [35,36]:

$$EAE(E) = \frac{\int_0^{E_0} \Phi_0(E) E \left(\frac{\mu_{en}(E)/\rho}{\mu_{att}(E)/\rho}\right) \left(1 - e^{-(\mu_{att}(E)/\rho)dW}\right) dE}{\int_0^{E_0} \Phi_0(E) E dE}, \quad (1)$$

where $\Phi_0(E)$ is the incident X-ray photon fluence on the scintillator; E is the photon energy; $\mu_{en}(E)/\rho$ is the corresponding total mass energy absorption coefficient; $\mu_{att}(E)/\rho$ is the radiation photon total mass attenuation coefficient; T is the thickness of the crystal; and the density is ρ (in g/cm^3) [37–39]. Coefficients data for lead fluoride elements were obtained from the National Institute of Standards and Technology (NIST) data using the XmuDat photon attenuation database software [40–42].

2.2. Experiments

Experiments were performed using X-ray excitation by a CPI Inc. CMP 200 DR X-ray generator and an IAE model RTM90HS X-ray unit, from 50 to 130 kVp. An additional 20 mm Al filter was used to simulate attenuation by the human body. All experiments were performed at room temperature, with short exposure time intervals (1 s) to keep exposure as low as possible and no visible degradation of transparency (aging effects) [43]. Furthermore, Tc-99m (140 keV) and I-131 (365 keV) were also used to irradiate the crystal sample.

2.2.1. Absolute Efficiency (AE) and Output Signal

The luminescence efficiency and the output signal were defined for a range of X-ray energies. An integrating sphere (Oriel 70451) was used to collect the incident light energy of the crystal [37]. A photomultiplier tube (PMT) (EMI 9798) was used as a biased photodiode to collect the light at the output port, and an electrometer (Model 6430 Keithley) was connected to detect its current [38]. A digital multimeter (RTI Piranha P100B) provided the radiation dose rates.

Absolute efficiency describing the light output power per incident X-ray exposure was defined as [44,45]:

$$AE = \eta_A = \frac{\dot{\Psi}_\lambda}{\dot{X}} = \left(\frac{i_{elec}}{S\eta_p \alpha_s c_g}\right) \dot{X}^{-1} \quad (2)$$

where S is the scintillator's irradiated area (in mm^2); i_{elec} is the current of the PMT (in pA); η_p is the photocathode's peak photosensitivity (pA W^{-1}); c_g is the geometric light collection efficiency of the experimental configuration; and α_s is the spectral matching factor connecting the emitted light spectrum of the scintillator and the spectral response of the photocathode. The units are: 1 EU = 1 μW m^{-2}/(mR s^{-1}).

By multiplying the AE by exposure, the output signal can be obtained [37]. The output signal is expressed (in μW m^{-2}).

2.2.2. X-ray Luminescence Efficiency (XLE)

XLE is a unitless quantity that characterizes energy-integrating detectors by quantifying the efficiency of the latter in converting X-rays to visible photons. XLE (η_Ψ) can be described as the ratio of the light energy flux produced by the crystal divided by the X-ray energy flux [35]:

$$\eta_\Psi = \Psi_\Lambda / \Psi_0 \quad (3)$$

3. Results

Figure 1 shows the energy absorption coefficients ($\mu_{en}(E)/\rho$) and the attenuation coefficients ($\mu_{att}(E)/\rho$) of PbF_2 and BGO for an energy range up to 400 keV. The corresponding X-ray experimental range of this study is up to 365 keV. The characteristic photoelectric absorption edges are also shown at the energy levels of ~13 keV, ~15 keV, and ~88 keV. From the calculated results shown in Figure 1, it can be depicted that PbF_2 seems to adequately absorb radiation with attenuation coefficient values higher than BGO across the examined

energy range. These results show a crystal that fulfills the stopping power criteria required in applications such as medical imaging.

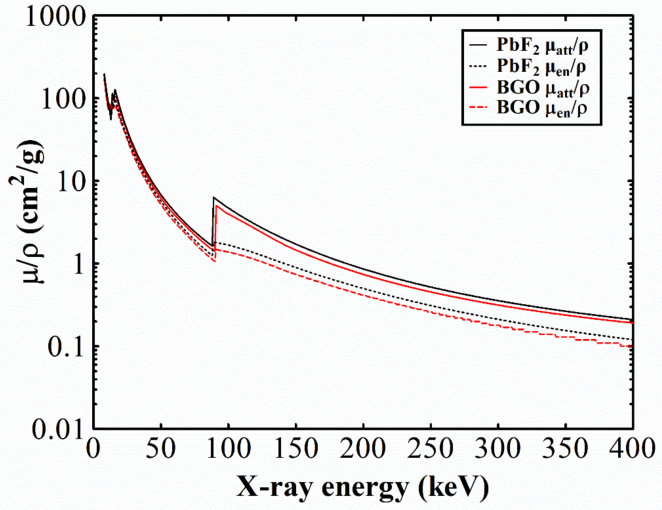

Figure 1. PbF_2 attenuation coefficients. For comparison, data for BGO are also shown.

Figure 2 shows the ratio of the attenuation coefficients (μ_{en}/μ_{att}) that is used in Equation (1). In this figure, one can see the steep reduction in the coefficients ratio μ_{en}/μ_{att} occuring at the energy levels at which characteristic energy is produced. For example, this effect is evident at ~88 keV, due to the characteristic k-edges of the material.

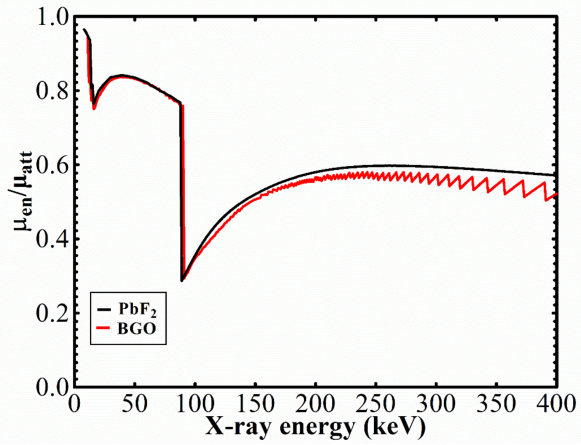

Figure 2. Attenuation coefficients ratio μ_{en}/μ_{att} of PbF_2 and BGO.

This effect contributes to the reduction in the energy absorption values of both materials. The reduction can be clearly shown after 90 kVp (Figure 3). In this figure, the EAE of PbF_2 is slightly higher than BGO up to 90 kVp. Thereafter, BGO shows slightly higher values. This change is also shown in Figure 2, in which the coefficients ratio of BGO overcomes PbF_2 in the k-edge energy level.

From the calculated results and the announced properties of PbF_2, further experimental investigation of the internal material properties was deemed appropriate in order to determine its suitability for application in radiographic imaging. Thus, Figure 4 shows the luminescence efficiency values of PbF_2 compared with a commercially available crystal used in PET scanners (BGO). Results are shown for the X-ray radiography and gamma ray energy ranges. However, whereas BGO values increased as the X-ray energy increased, the corresponding values of PbF_2 decreased in the whole X-ray energy range, with a minimum value of 0.03 EU at 71 keV. At this energy, BGO showed its maximum, with a value of 3.35 EU. In the gamma ray energy range, BGO [46] showed lower AE values, whereas,

at the energy of 140 keV (Tc-99m), PbF_2 showed the maximum AE value (0.59 EU). The corresponding value for BGO was 1.96 EU. For higher gamma ray energies (365 keV I-131), the absolute efficiency values for the two materials were 0.1 EU for PbF_2 and 1.35 EU for BGO. This negligible output of PbF_2 has been previously depicted [40,41].

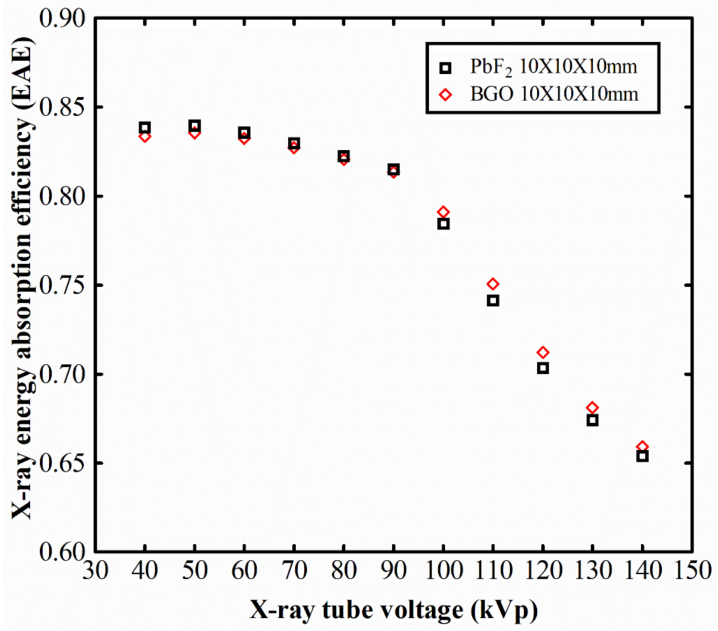

Figure 3. Energy absorption efficiency of PbF_2 and BGO.

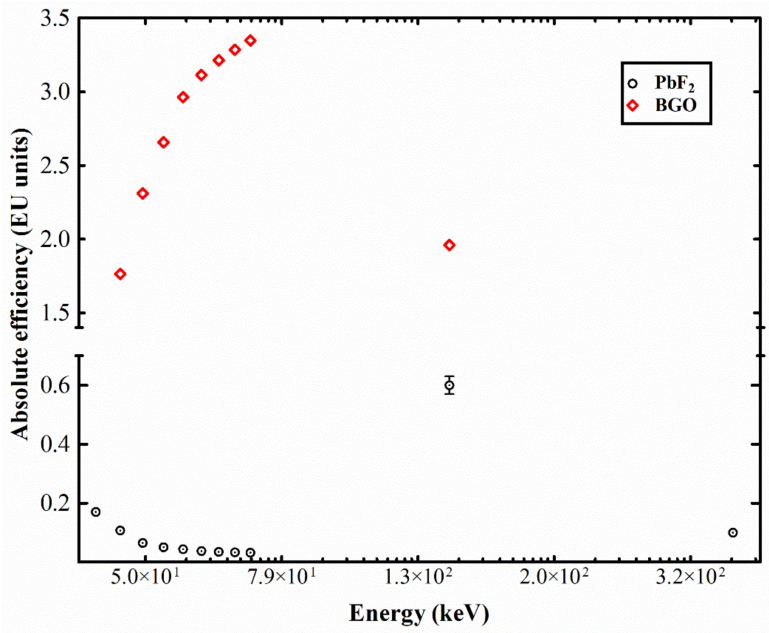

Figure 4. X-ray absolute luminescence efficiency of PbF_2 and BGO crystals in the X-ray (42–71 keV) and nuclear medicine (140 keV Tc-99m, 365 keV I-131) energy ranges.

Regarding the output signal (Figure 5), a linear relationship was observed for both crystals in the X-ray energy range, with BGO having an R^2 value of 0.9986 and PbF_2, a value of 0.9875. The differences between the slope (i.e., detector optical gain) values (3.37 for BGO and 0.03 for PbF_2) reveal the unsuitability of PbF_2 for medical imaging applications in the radiographic energy range, despite the lower density of BGO (7.13 g/cm^3) compared to PbF_2 (7.77 g/cm^3).

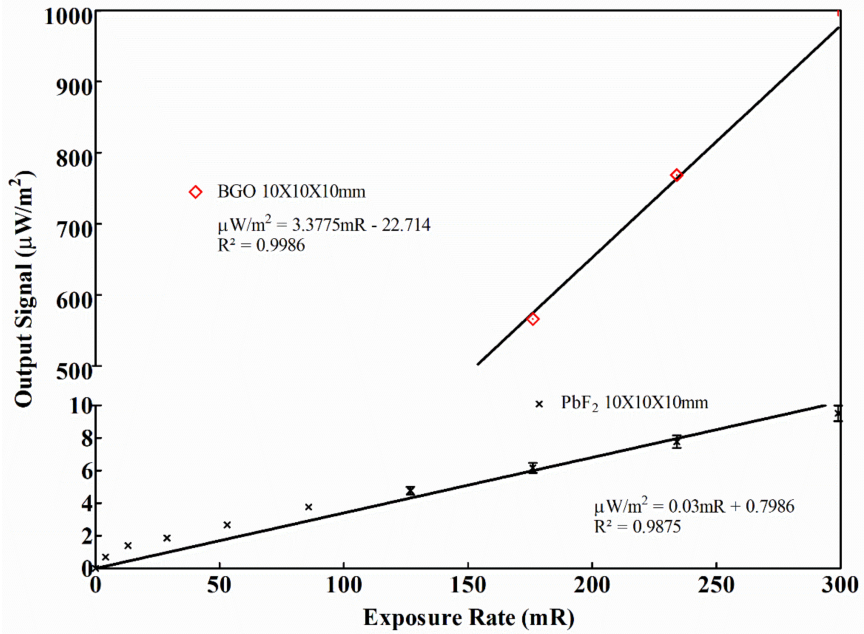

Figure 5. Output signal of PbF_2 and BGO crystals in the X-ray exposure rate range 0–299 mR/s.

XLE values of PbF_2 are shown in Figure 6, against the corresponding values for BGO. PbF_2 XLE values started from 11.6×10^{-5} at 42.39 keV and decreased constantly thereafter in the whole radiographic range. The corresponding maximum value of BGO in the radiographic range was 11×10^{-4} at 53 keV. Under Tc-99m gamma ray excitation, the XLE of PbF_2 showed a local maximum (12.6×10^{-5} at 140 keV). In this energy, BGO had an XLE value of 55.1×10^{-5}. Under I-131 gamma ray energy (365 keV), the X-ray luminescence efficiency of PbF_2 dropped to 3.4×10^{-5}, whereas the corresponding BGO value was 45.4×10^{-5}. Generally, XLE values follow a similar trend to the absolute efficiency, except for the fact that the differences in shape of AE and XLE curves are attributed to the fact that the LE is not affected by the X-ray fluence to exposure conversion factor.

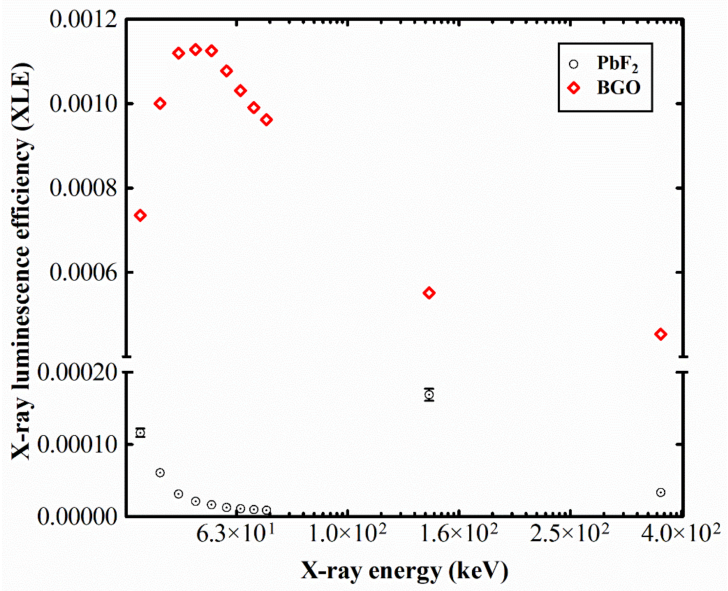

Figure 6. X-ray luminescence efficiency of PbF_2 and BGO crystals in the X-ray (42–71 keV) and nuclear medicine (140 keV Tc-99m, 365 keV I-131) energy ranges.

4. Discussion

In recent years, a number of articles have depicted the potentiality of PbF_2 for use in various applications, among them medical imaging [20,47–49]. The single crystal PbF_2 has been extensively studied as a Cherenkov radiator for electromagnetic calorimetry. Thus, it would be very useful for many medical applications if it could be scintillated with a reasonable light output and a short decay time. Furthermore, the X-ray luminescence of orthorhombic PbF_2 has been previously reported at room temperatures, even with the low energy excitation that can be found in mammography and general radiography (30–50 kV) [32,33]. The provided high density value (ρ = 7.77), high atomic number (Z = 82), its transparency in near-UV radiation, and the low cost of this material, along with references for possible applications in medical imaging, intrigues the scientific curiosity for further investigation to verify or not the above-mentioned allegations [43,50]. Despite these advantages, during this study on the PbF_2 crystal, the produced light output (X-ray energy range) was extremely low [51].

However, all results converge on the conclusion that PbF_2 scintillation is quenched in the X-ray and gamma ray energy ranges in room temperature conditions. This is in accordance with previously published works, in which it was stated that PbF_2 emission was limited to a restricted number of photons/MeV of deposited energy [32,44]. Lead fluoride can be found in orthorhombic (space group 62, D_{2h}^{16}, cotunnite-type) and cubic (space group 225, O_h^5, fluorite-type) crystalline phases [52,53]. The properties of binary lead halides such as PbF_2 strongly depend on the presence of self-trapped carriers. These defects (self-trapped electrons, STEL, or self-trapped holes, STH) show low stability, and only 0.1 eV is enough for their delocalization, even at very low temperatures. The strong hole-trapping on Pb results in the extremely low light output of PbF_2. The Pb^{2+} ion belongs to the family of the $^6S_2$ ions. These ions are characterized by excitations from $^1S_0$ ground state to the $^3P_1$, $^3P_2$, and $^1P_1$ excited states. In this configuration, a relatively small lattice parameter is observed (5.94 A), and the Pb–Pb distance of 4 A results in a large wave function overlap and energy propagation through the crystal lattice [51,54].

Luminescence can be observed at liquid helium temperatures, depending upon the structure of the material (cubic or orthorhombic), since the very small energy of the self-trapped electrons (0.1 eV) eliminates the possibility for experimental light detection at higher temperatures [53,55]. The luminescence spectra of PbF_2 have been reported at temperatures of −271 °C, with a maximum at 2.2 eV [45]; however, luminescence is negligible for temperatures above −123 °C [53].

In order to avoid the hole-trapping, which results in extremely low absolute efficiency (AE), it would be useful to further examine the luminescence spectra of PbF_2 at temperatures near absolute zero (i.e., −271 °C) [55].

5. Conclusions

This research aimed to examine the possible application of the PbF_2 crystal to radiographic and nuclear medicine imaging. To this end, luminescence and scintillation properties of this material were examined in these energy ranges. The theoretical results regarding the attenuation coefficients and the energy absorption efficiency, in combination with the high stopping power of the material, showed promise, comparable to the established BGO crystal and even slightly higher. However, the experimental findings regarding the luminescence output of PbF_2 showed a completely different reality, with values significantly lower than BGO and, in every case, unacceptable for medical imaging applications.

Author Contributions: Conceptualization, V.N. and C.M.; data curation, V.N., D.L., C.M., N.K. and G.F.; formal analysis, V.N., C.M., D.L., N.K. and A.B.; investigation, V.N., D.L., G.S., C.M., N.K., I.V. and G.F.; methodology, V.N., D.L., C.M., G.S., N.K., I.V. and G.F.; project administration, C.M. and I.V.; resources, I.V. and A.B.; software, D.L.; supervision, C.M. and I.V.; validation, N.K. and G.F.; visualization, C.M. and I.V.; writing—original draft, V.N., D.L., I.K. and C.M.; writing—review and editing, N.K., I.K. and C.M. All authors have read and agreed to the published version of the manuscript.

Funding: This research received no external funding.

Institutional Review Board Statement: Not applicable.

Informed Consent Statement: Not applicable.

Data Availability Statement: Data are contained within the article.

Conflicts of Interest: The authors declare no conflict of interest.

References

1. Chen, Q.; Wu, J.; Ou, X.; Huang, B.; Almutlaq, J.; Zhumekenov, A.A.; Guan, X.; Han, S.; Liang, L.; Yi, Z.; et al. All-Inorganic Perovskite Nanocrystal Scintillators. *Nature* **2018**, *561*, 88–93. [CrossRef] [PubMed]
2. Büchele, P.; Richter, M.; Tedde, S.F.; Matt, G.J.; Ankah, G.N.; Fischer, R.; Biele, M.; Metzger, W.; Lilliu, S.; Bikondoa, O.; et al. X-Ray Imaging with Scintillator-Sensitized Hybrid Organic Photodetectors. *Nat. Photonics* **2015**, *9*, 843–848. [CrossRef]
3. Kim, Y.C.; Kim, K.H.; Son, D.-Y.; Jeong, D.-N.; Seo, J.-Y.; Choi, Y.S.; Han, I.T.; Lee, S.Y.; Park, N.-G. Printable Organometallic Perovskite Enables Large-Area, Low-Dose X-Ray Imaging. *Nature* **2017**, *550*, 87–91. [CrossRef] [PubMed]
4. Gupta, S.K.; Zuniga, J.P.; Abdou, M.; Thomas, M.P.; De Alwis Goonatilleke, M.; Guiton, B.S.; Mao, Y. Lanthanide-Doped Lanthanum Hafnate Nanoparticles as Multicolor Phosphors for Warm White Lighting and Scintillators. *Chem. Eng. J.* **2020**, *379*, 122314. [CrossRef]
5. Hajagos, T.J.; Liu, C.; Cherepy, N.J.; Pei, Q. High-Z Sensitized Plastic Scintillators: A Review. *Adv. Mater.* **2018**, *30*, 1706956. [CrossRef]
6. Ichikawa, J.; Kominami, H.; Hara, K.; Kakihana, M.; Matsushima, Y. Electronic Structure Calculation of Cr^{3+} and Fe^{3+} in Phosphor Host Materials Based on Relaxed Structures by Molecular Dynamics Simulation. *Technologies* **2022**, *10*, 56. [CrossRef]
7. Huang, X.; Wang, Y.; Zhang, P.; Su, Z.; Xu, J.; Xin, K.; Hang, Y.; Zhu, S.; Yin, H.; Li, Z.; et al. Efficiently Strengthen and Broaden 3 μm Fluorescence in PbF_2 Crystal by Er^{3+}/Ho^{3+} as Co-Luminescence Centers and Pr^{3+} Deactivation. *J. Alloys Compd.* **2019**, *811*, 152027. [CrossRef]
8. Xia, X.; Hu, X.; Zou, J. Dual-Energy x-Ray Computed Tomography Study Based on CsI:Tl and LYSO:Ce Scintillator Combination. *J. Appl. Phys.* **2021**, *130*, 234902. [CrossRef]
9. Kim, C.; Lee, W.; Melis, A.; Elmughrabi, A.; Lee, K.; Park, C.; Yeom, J.-Y. A Review of Inorganic Scintillation Crystals for Extreme Environments. *Crystals* **2021**, *11*, 669. [CrossRef]
10. Lecoq, P.; Gektin, A.; Korzhik, M. *Inorganic Scintillators for Detector Systems: Physical Principles and Crystal Engineering*, 2nd ed.; Particle Acceleration and Detection; Springer International Publishing: New York, NY, USA, 2017; ISBN 978-3-319-45521-1.
11. Popov, A.I.; Chernov, S.A.; Trinkler, L.E. Time-Resolved Luminescence of CsI-Tl Crystals Excited by Pulsed Electron Beam. *Nucl. Instrum. Methods Phys. Res. Sect. B Beam Interact. Mater. At.* **1997**, *122*, 602–605. [CrossRef]
12. Michail, C.; Kalyvas, N.; Bakas, A.; Ninos, K.; Sianoudis, I.; Fountos, G.; Kandarakis, I.; Panayiotakis, G.; Valais, I. Absolute Luminescence Efficiency of Europium-Doped Calcium Fluoride (CaF_2:Eu) Single Crystals under X-Ray Excitation. *Crystals* **2019**, *9*, 234. [CrossRef]
13. van Eijk, C.W.E. Inorganic Scintillators in Medical Imaging Detectors. *Nucl. Instrum. Methods Phys. Res. Sect. Accel. Spectrometers Detect. Assoc. Equip.* **2003**, *509*, 17–25. [CrossRef]
14. Kalavathi, P.; Senthamilselvi, M.; Prasath, V.B.S. Review of Computational Methods on Brain Symmetric and Asymmetric Analysis from Neuroimaging Techniques. *Technologies* **2017**, *5*, 16. [CrossRef]
15. Jung, J.; Jang, Y.; Kim, M.; Kim, H. Types/Applications of Photoacoustic Contrast Agents: A Review. *Photonics* **2021**, *8*, 287. [CrossRef]
16. Hatefi Hesari, S.; Haque, M.A.; McFarlane, N. A Comprehensive Survey of Readout Strategies for SiPMs Used in Nuclear Imaging Systems. *Photonics* **2021**, *8*, 266. [CrossRef]
17. Bryant, P.A. Communicating Radiation Risk: The Role of Public Engagement in Reaching ALARA. *J. Radiol. Prot.* **2021**, *41*, S1–S8. [CrossRef]
18. Shevelev, V.S.; Ishchenko, A.V.; Vanetsev, A.S.; Nagirnyi, V.; Omelkov, S.I. Ultrafast Hybrid Nanocomposite Scintillators: A Review. *J. Lumin.* **2022**, *242*, 118534. [CrossRef]
19. Jones, T.; Townsend, D.W. History and Future Technical Innovation in Positron Emission Tomography. *J. Med. Imaging* **2017**, *4*, 011013. [CrossRef]
20. Consuegra, D.; Korpar, S.; Križan, P.; Pestotnik, R.; Razdevšek, G.; Dolenec, R. Simulation Study to Improve the Performance of a Whole-Body PbF_2 Cherenkov TOF-PET Scanner. *Phys. Med. Biol.* **2020**, *65*, 055013. [CrossRef]
21. Rausch, I.; Ruiz, A.; Valverde-Pascual, I.; Cal-González, J.; Beyer, T.; Carrio, I. Performance Evaluation of the Vereos PET/CT System According to the NEMA NU2-2012 Standard. *J. Nucl. Med.* **2019**, *60*, 561–567. [CrossRef]
22. Grant, A.M.; Deller, T.W.; Khalighi, M.M.; Maramraju, S.H.; Delso, G.; Levin, C.S. NEMA NU 2-2012 Performance Studies for the SiPM-Based ToF-PET Component of the GE SIGNA PET/MR System. *Med. Phys.* **2016**, *43*, 2334–2343. [CrossRef] [PubMed]
23. van Sluis, J.; de Jong, J.; Schaar, J.; Noordzij, W.; van Snick, P.; Dierckx, R.; Borra, R.; Willemsen, A.; Boellaard, R. Performance Characteristics of the Digital Biograph Vision PET/CT System. *J. Nucl. Med.* **2019**, *60*, 1031–1036. [CrossRef]
24. Lecoq, P. Pushing the Limits in Time-of-Flight PET Imaging. *IEEE Trans. Radiat. Plasma Med. Sci.* **2017**, *1*, 473–485. [CrossRef]

25. Lecoq, P.; Morel, C.; Prior, J.O.; Visvikis, D.; Gundacker, S.; Auffray, E.; Križan, P.; Turtos, R.M.; Thers, D.; Charbon, E.; et al. Roadmap toward the 10 Ps Time-of-Flight PET Challenge. *Phys. Med. Ampmathsemicolon Biol.* **2020**, *65*, 21RM01. [CrossRef] [PubMed]
26. Dolenec, R.; Chagani, H.; Korpar, S.; Križan, P.; Pestotnik, R.; Stanovnik, A.; Verheyden, R. Time-of-Flight with Photonis Multi-Channel MCP-PMT Using MCP Signal. In Proceedings of the 2009 IEEE Nuclear Science Symposium Conference Record (NSS/MIC), Orlando, FL, USA, 25–31 October 2009; pp. 1558–1560.
27. Korpar, S.; Dolenec, R.; Križan, P.; Pestotnik, R.; Stanovnik, A. Study of a Cherenkov TOF-PET Module. *Nucl. Instrum. Methods Phys. Res. Sect. Accel. Spectrometers Detect. Assoc. Equip.* **2013**, *732*, 595–598. [CrossRef]
28. Brunner, S.E.; Gruber, L.; Marton, J.; Suzuki, K.; Hirtl, A. Studies on the Cherenkov Effect for Improved Time Resolution of TOF-PET. *IEEE Trans. Nucl. Sci.* **2014**, *61*, 443–447. [CrossRef]
29. Kurosawa, S.; Yanagida, T.; Yokota, Y.; Yoshikawa, A. Crystal Growth and Scintillation Properties of Fluoride Scintillators. *IEEE Trans. Nucl. Sci.* **2012**, *59*, 2173–2176. [CrossRef]
30. Li, C.; Lin, J. Rare Earth Fluoride Nano-/Microcrystals: Synthesis, Surface Modification and Application. *J. Mater. Chem.* **2010**, *20*, 6831–6847. [CrossRef]
31. Consuegra, D.; Korpar, S.; Pestotnik, R.; Krivzan, P.; Dolenec, R. MCP-PMT Timing at Low Light Intensities with a DRS 4 Evaluation Board. *Nucleus* **2019**, *65*, 42–46.
32. Alokhina, M.; Canot, C.; Bezshyyko, O.; Kadenko, I.; Tauzin, G.; Yvon, D.; Sharyy, V. Simulation and Optimization of the Cherenkov TOF Whole-Body PET Scanner. *Nucl. Instrum. Methods Phys. Res. Sect. Accel. Spectrometers Detect. Assoc. Equip.* **2018**, *912*, 378–381. [CrossRef]
33. Kozma, P.; Bajgar, R.; Kozma, P. Radiation Resistivity of PbF_2 Crystals. *Nucl. Instrum. Methods Phys. Res. Sect. Accel. Spectrometers Detect. Assoc. Equip.* **2002**, *484*, 149–152. [CrossRef]
34. PbF2—Lead Fluoride Scintillator Crystal. Available online: https://www.advatech-uk.co.uk/pbf2.html (accessed on 8 October 2022).
35. Egorov, V.K.; Klassen, N.V.; Negrii, V.D.; Prokopenko, V.M.; Shmurak, S.Z.; Sinitzin, V.V.; Solov'ev, A.V. Comparative Studies of Optical Spectra in PbF_2 at Different Excitations. *MRS Online Proc. Libr.* **1994**, *348*, 265–269. [CrossRef]
36. Jiang, H.; Orlando, R.; Blanco, M.A.; Pandey, R. First-Principles Study of the Electronic Structure of PbF_2 in the Cubic, Orthorhombic, and Hexagonal Phases. *J. Phys. Condens. Matter* **2004**, *16*, 3081–3088. [CrossRef]
37. Korpar, S.; Dolenec, R.; Križan, P.; Pestotnik, R.; Stanovnik, A. Study of TOF PET Using Cherenkov Light. *Nucl. Instrum. Methods Phys. Res. Sect. Accel. Spectrometers Detect. Assoc. Equip.* **2011**, *654*, 532–538. [CrossRef]
38. Michail, C.; Koukou, V.; Martini, N.; Saatsakis, G.; Kalyvas, N.; Bakas, A.; Kandarakis, I.; Fountos, G.; Panayiotakis, G.; Valais, I. Luminescence Efficiency of Cadmium Tungstate ($CdWO_4$) Single Crystal for Medical Imaging Applications. *Crystals* **2020**, *10*, 429. [CrossRef]
39. Boone, J.M. X-Ray Production, Interaction, and Detection in Diagnostic Imaging. *Handb. Med. Imaging* **2000**, *PM79*, 1–78. [CrossRef]
40. Storm, L.; Israel, H.I. Photon Cross Sections from 1 KeV to 100 MeV for Elements Z=1 to Z=100. *At. Data Nucl. Data Tables* **1970**, *7*, 565–681. [CrossRef]
41. Hubbell, J.H.; Seltzer, S.M. *Tables of X-Ray Mass Attenuation Coefficients and Mass Energy-Absorption Coefficients 1 KeV to 20 MeV for Elements Z = 1 to 92 and 48 Additional Substances of Dosimetric Interest*; National Institute of Standards and Technology: Gaithersburg, MD, USA, 1995.
42. International Atomic Energy Agency. *XMuDat: Photon Attenuation Data on PC Version 101 of August 1998 Summary Documentation*; International Atomic Energy Agency (IAEA): Vienna, Austria, 1998.
43. Loyd, M.; Pianassola, M.; Hurlbut, C.; Shipp, K.; Zaitseva, N.; Koschan, M.; Melcher, C.L.; Zhuravleva, M. Accelerated Aging Test of New Plastic Scintillators. *Nucl. Instrum. Methods Phys. Res. Sect. Accel. Spectrometers Detect. Assoc. Equip.* **2020**, *949*, 162918. [CrossRef]
44. Linardatos, D.; Konstantinidis, A.; Valais, I.; Ninos, K.; Kalyvas, N.; Bakas, A.; Kandarakis, I.; Fountos, G.; Michail, C. On the Optical Response of Tellurium Activated Zinc Selenide ZnSe:Te Single Crystal. *Crystals* **2020**, *10*, 961. [CrossRef]
45. Saatsakis, G.; Kalyvas, N.; Michail, C.; Ninos, K.; Bakas, A.; Fountzoula, C.; Sianoudis, I.; Karpetas, G.E.; Fountos, G.; Kandarakis, I.; et al. Optical Characteristics of ZnCuInS/ZnS (Core/Shell) Nanocrystal Flexible Films Under X-Ray Excitation. *Crystals* **2019**, *9*, 343. [CrossRef]
46. Valais, I.G.; Michail, C.M.; David, S.L.; Liaparinos, P.F.; Fountos, G.P.; Paschalis, T.V.; Kandarakis, I.S.; Panayiotakis, G.S. Comparative Investigation of Ce^{3+} Doped Scintillators in a Wide Range of Photon Energies Covering X-Ray CT, Nuclear Medicine and Megavoltage Radiation Therapy Portal Imaging Applications. *IEEE Trans. Nucl. Sci.* **2010**, *57*, 3–7. [CrossRef]
47. Kurosawa, S.; Kochurikhin, V.V.; Yamaji, A.; Yokota, Y.; Kubo, H.; Tanimori, T.; Yoshikawa, A. Development of a Single Crystal with a High Index of Refraction. *Nucl. Instrum. Methods Phys. Res. Sect. Accel. Spectrometers Detect. Assoc. Equip.* **2013**, *732*, 599–602. [CrossRef]
48. Ren, G.; Shen, D.; Wang, S.; Yin, Z. Structural Defects and Characteristics of Lead Fluoride (PbF_2) Crystals Grown by Non-Vacuum Bridgman Method. *J. Cryst. Growth* **2002**, *243*, 539–545. [CrossRef]

49. Eriksson, L.; Cho, S.; Aykac, M.; Melcher, C.L.; Conti, M.; Eriksson, M.; Michel, C. Comparison of Count Rate Sensitivity Performance for a LSO-TOF System with a Cherenkov Radiation Based PbF_2-TOF System. In Proceedings of the 2012 IEEE Nuclear Science Symposium and Medical Imaging Conference Record (NSS/MIC), Anaheim, CA, USA, 29 October–3 November 2012; pp. 3108–3111.
50. Munafò, M.R.; Nosek, B.A.; Bishop, D.V.M.; Button, K.S.; Chambers, C.D.; Percie du Sert, N.; Simonsohn, U.; Wagenmakers, E.-J.; Ware, J.J.; Ioannidis, J.P.A. A Manifesto for Reproducible Science. *Nat. Hum. Behav.* **2017**, *1*, 0021. [CrossRef]
51. Anderson, D.F.; Kierstead, J.A.; Lecoq, P.; Stoll, S.; Woody, C.L. A Search for Scintillation in Doped and Orthorhombic Lead Fluoride. *Nucl. Instrum. Methods Phys. Res. Sect. Accel. Spectrometers Detect. Assoc. Equip.* **1994**, *342*, 473–476. [CrossRef]
52. Achenbach, P.; Baunack, S.; Grimm, K.; Hammel, T.; von Harrach, D.; Ginja, A.L.; Maas, F.E.; Schilling, E.; Ströher, H. Measurements and Simulations of Cherenkov Light in Lead Fluoride Crystals. *Nucl. Instrum. Methods Phys. Res. Sect. Accel. Spectrometers Detect. Assoc. Equip.* **2001**, *465*, 318–328. [CrossRef]
53. Mastrikov, Y.A.; Chuklina, N.G.; Sokolov, M.N.; Popov, A.I.; Gryaznov, D.V.; Kotomin, E.A.; Maier, J. Small Radius Electron and Hole Polarons in PbX_2 (X = F, Cl, Br) Crystals: A Computational Study. *J. Mater. Chem. C* **2021**, *9*, 16536–16544. [CrossRef]
54. Derenzo, S.E.; Weber, M.J. Prospects for First-Principle Calculations of Scintillator Properties. *Nucl. Instrum. Methods Phys. Res. Sect. Accel. Spectrometers Detect. Assoc. Equip.* **1999**, *422*, 111–118. [CrossRef]
55. Alov, D.L.; Rybchenko, S.I. Luminescence Kinetics Of Orthorhombic PbF_2. *MRS Online Proc. Libr.* **1994**, *348*, 271–275. [CrossRef]